# Enhanced Molecular Level Dispersion and Interface Bonding at Low Loading of Modified Graphene Oxide To Fabricate Super Nylon 12 Composites

Sunanda Roy,[†,§] Xiuzhi Tang,[†,§] Tanya Das,[‡] Liying Zhang,[†] Yongmei Li,[†] Sun Ting,[†] Xiao Hu,*[,†] and C. Y. Yue*[,‡]

[†]School of Materials Science and Engineering, Nanyang Technological University, Singapore 639798

[‡]School of Mechanical and Aerospace Engineering, Nanyang Technological University, Singapore 639798
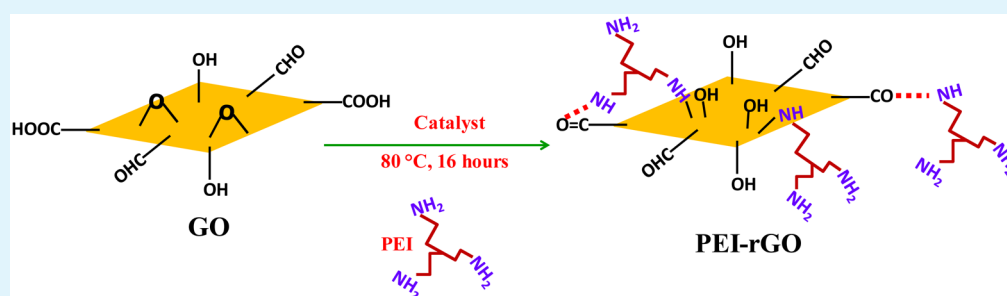
ABSTRACT: Development of advanced graphene based polymer composites is still confronted with severe challenges due to its poor dispersion caused by restacking, weak interface bonding, and incompatibility with polymer matrices which suppress exertion of the actual potential of graphene sheets in composites. Here, we have demonstrated an efficient chemical modification process with polyethylenimine (PEI) to functionalize graphene oxide which can overcome the above-mentioned drawbacks and also can remarkably increase the overall strength of the nylon 12 composites even at very low graphene loading. Chemical modification was analyzed by various surface characterizations including X-ray photoelectron spectroscopy, Fourier transform infrared spectroscopy, and X-ray diffraction. Addition of only 0.25 and 0.35 wt % modified GO showed 37% and 54% improvement in tensile strength and 65% and 74% in Young's modulus, respectively, compared with that of the neat polymer. The dynamic mechanical analysis showed ∼39% and 63% increment in storage modulus of the nanocomposites. Moreover, the nanocomposites exhibited significantly high thermal stability (∼15 °C increment by only 0.35 wt %) as compared to neat polymer. Furthermore, the composites rendered outstanding resistance against various chemicals.

KEYWORDS: graphene, PEI, XPS, nanocomposite, tensile strength, Young's modulus

1. INTRODUCTION

The discovery of graphene[1] brings a new era in nanotechnology and many other fields of materials science and engineering because of its high specific surface area (2600 m^2/g) and extreme electrical, thermal, mechanical, and chemical properties.[2−7] On the basis of such unique properties, recently tremendous research interests have grown on the development of useful polymer composites based on graphene material. It has been noticed that among all graphene-based materials including graphene nanoplatelets (GNPs), graphene nanosheets (GNSs), and graphene oxide (GO), GO possesses the widest potential because of its unique chemical structures that contain a wide variety of oxygen functional groups (e.g., hydroxyl, epoxide, carbonyl, and carboxylic acid groups) both on the basal planes and at the edges of graphene oxide sheets.[8,9] Moreover, this can be further tailored to produce homogeneous colloidal suspensions in various solvents as well as to influence the properties of graphene-based polymer composites. In recent years, various attempts have been made to fabricate polymer/graphene or polymer/GO nanocomposites using chemically modified GO to improve the solubility and dispersion of GO sheets in polymer systems. The modification of GO sheets is expected to play a key role in tailoring its structure and properties and also enables development of novel polymer/graphene composites with enhanced functional properties. However, these improvements largely depend on the synthesis of well exfoliated and high-quality funtionalized graphene sheets. Hence, an appropriate surface functionalization is very important to achieve. Fang et al. demonstrated[10] the preparation of functionalized GO/polystyrene (PS) composites via a long chemical process including diazonium addition followed by atom transfer radical polymerization (ATRP). They noticed about 70% and 57% increase in the tensile strength and Young's modulus by addition of 0.9 wt % modified graphene nanosheets. Liang et al.[11] prepared poly(vinyl alcohol) (PVA)/GO composites with a 76% increase in tensile
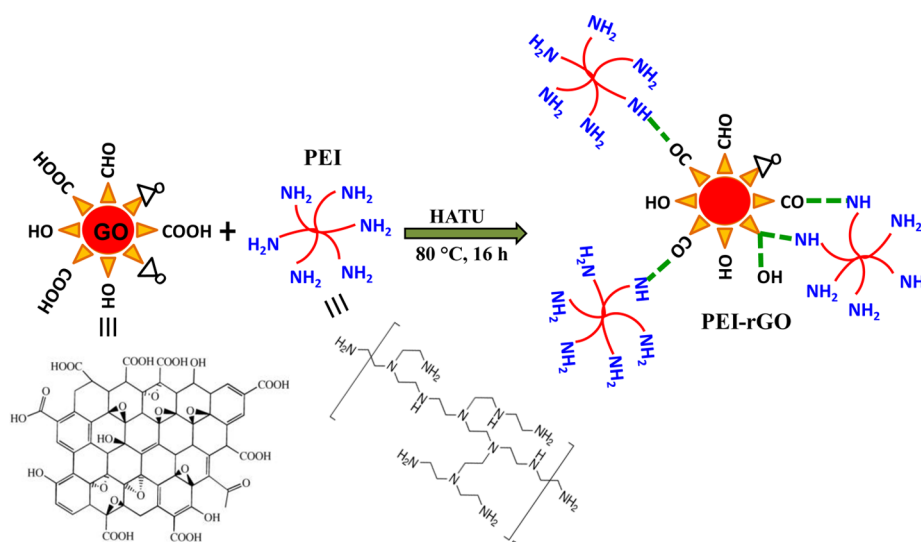
Figure 1. Schematic representation of the preparation of amine modified graphene oxide (PEI-rGO) and their various interaction sites.

strength and a 62% improvement of Young's modulus at a loading of 0.7 wt % graphene oxide. Huang et al.[12] reported the preparation of chemically modified graphene oxide/polyimide (MG/PI) composites. The GO was modified for a long period of time (~3−4 days) with a number of chemical agents to accomplish the desired surface grafting. The resulting composites show ~40% and 42% increase in tensile strength and Young's modulus by addition of 2 wt % MG. Yuan et al.[13] prepared octadecylamine-modified graphene/PMMA composites by in situ bulk-polymerization process. The composites containing 0.5 wt % modified graphene showed only ~30−31% improvement in tensile strength, while the onset decomposition temperature was increased by only 7 °C. Gonçalves et al.[14] modified the surface of GO with PMMA chains via ATRP and then used it to prepare PMMA based composites. They noticed about 18% and 16% enhancement in the tensile strength and Young's modulus by incorporation of 1 wt % PMMA functionalized GO. Very recently, Park et al.[15] also demonstrated the fabrication of iodo functionalized graphene/polyimide (PI) composites via in situ polymerization process. The composites exhibited ~64% and 170% enhancement in tensile strength and Young's modulus as compared to the pure PI with addition of 0.5 wt % of iodographene. Therefore, from the above it is clear that surface modification of graphene oxide is necessary to improve the performance of the end products. However, the molecular-level dispersion and maximum interfacial interaction between the graphene nanosheets and the host matrix at low loading that allows strong, durable, and cost-efficient composites are yet very challenging.

Therefore, in the present article, we attempt to modify GO in such a way that addition of a very small amount of GO can provide tremendous mechanical strength, dynamic mechanical and thermal properties of the composites through their excellent dispersion and interfacial interaction with polymer matrix. The GO was chemically modified with polyethylenimine (PEI). Nylon 12 was chosen as polymer matrix, since it has high performance applications[16−18] due to its several superior properties such as low moisture absorption, high pressure resistance, very high impact and notched impact strengths, high mechanical performance at extreme temperatures, exceptional resistance to abrasion and stress cracking, better chemical resistance, high ultraviolet (UV) resistance, and

high processability. Composites were prepared by melt mixing method, as it is a simple, eco-friendly, industrially compatible process and can produce high performance polymer composites on a commercial scale at low cost. The PEI was selectively chosen because it contains multiple reactive amine sites and can effectively increase the hydrogen bonding points with the functional groups on GO surface which brings extra benefits to enhance the dispersion and interaction of graphene sheets in Nylon matrix.

2. EXPERIMENTAL SECTION

2.1. Materials. Flaky graphite powders (300 mesh) were provided by Huadong Graphite Factory (Pingdu, China). Concentrated sulfuric acid, concentrated hydrochloric acid, potassium permanganate and sodium nitrate were of analytical grade and purchased from Beijing Chemical Factory (China). Polyethylenimine (PEI, branched) with an average molecular weight of 800 and N,N-dimethylformamide (anhydrous) were bought from Sigma-Aldrich company. The condensing agent 1-[bis(dimethylamino)methylene]-1H-1,2,3-triazolo[4,5-b]pyridinium 3-oxide hexafluorophosphate (HATU) was commercially obtained from Merck chemicals company. All the above chemicals were used without further purification. Nylon 12 pellets used in this experiment were purchased from Sigma-Aldrich, Singapore. The pellet size was 5 mm and density was 1.01 g/mL at 25 °C. Prior to mixing, the Nylon pellets were dried in a vacuum oven for 6 h at 70 °C to remove residual moisture.

2.2. Preparation of GO and Functionalized PEI-rGO. Graphene oxide was synthesized by a modified Hummers method from graphite based on the earlier report.[19] The as-synthesized GO with a weight of 50 mg was dispersed into 100 mL of deionized water and treated in a bath sonicator for 1.5 h to form stable GO suspension. In nitrogen atmosphere, PEI (12.5 g) and HATU (5 mg) were then added into the mixture and the reaction was conducted at 80 °C for 16 h. The solids were separated by filtration and washed by large amounts of water and methanol repeatedly. Then it was freeze-dried overnight to obtain the final product PEI-rGO (PEI-reduced GO). The schematic representation of the functionalization is shown in Figure 1.

2.3. Preparation of Nylon 12/ PEI-rGO Nanocomposites. Nylon 12 composites containing 0.25, 0.35 wt % of PEI-rGO were prepared by melt mixing using a micromixer (HAAKE MiniLab), equipped with two counter-rotating screws at a temperature of 183 °C with a screw speed of 80 rpm for 7 min under N₂ gas flow to avoid the degradation of nylon. Film samples (~0.30 mm) were prepared by compression molding in a hot press at a temperature of 183 °C with a holding pressure of ~10 MPa for 3 min.
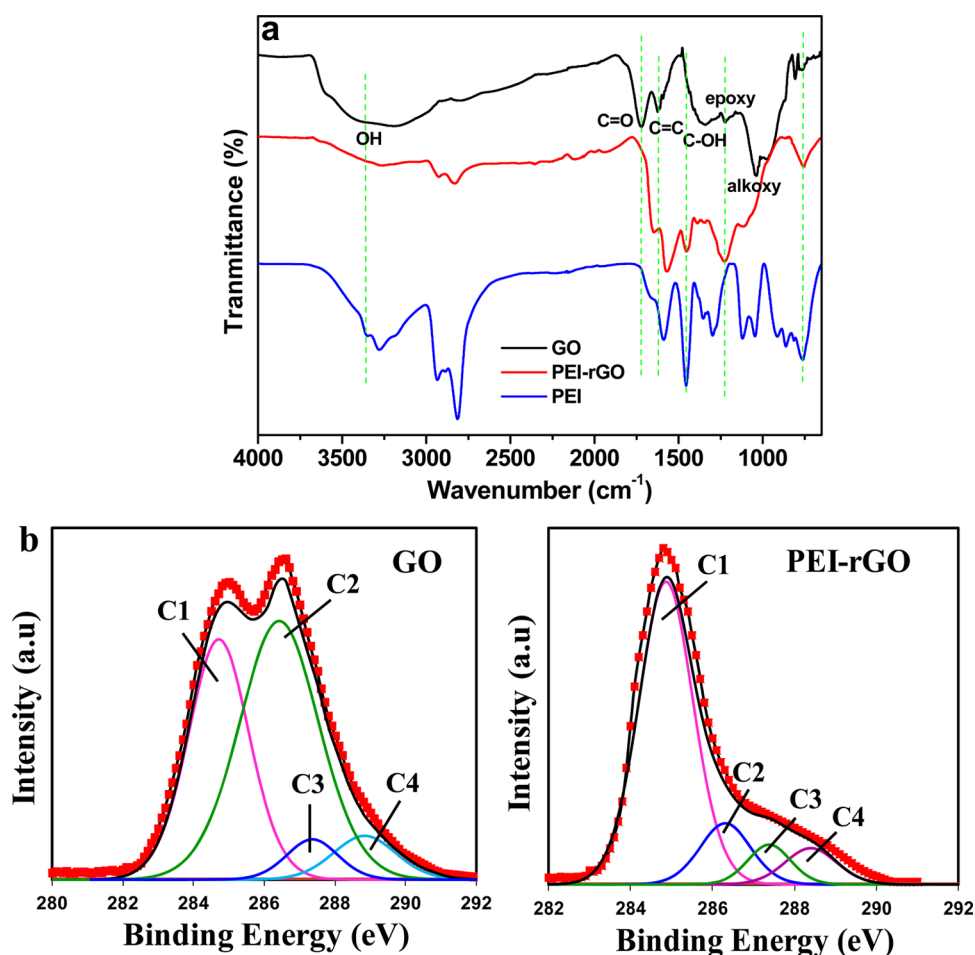
Figure 2. (a) FT-IR and (b) C 1s high resolution XPS spectra of GO and PEI-rGO.

2.4. Characterizations. Fourier transform infrared spectroscopy (FTIR) spectra for GO and PEI-rGO were recorded using a PerkinElmer GX FTIR spectrometer in transmission mode (KBr pellet). X-ray photoelectron spectroscopy (XPS) measurement was conducted with monochromatic Al Kα as an X-ray excitation source. The Raman spectra were measured by alpha300 R WITec confocal Raman microscope to investigate the structural changes of GO and GO-PEI. X-ray diffraction (XRD) patterns of the samples were obtained by a Bruker D8 powder X-ray diffractometer. Tensile test was conducted using an Instron machine (Instron Micro Tester 5848) at room temperature with crosshead speed of 50 mm/min. Specimens for tensile tests (dog bone shape) were prepared following the ASTM D638-V method. The morphology of graphene and fractured surface of nylon 12 composites was determined with a JEOL 6400F field emission scanning microscope (FESEM). Dynamic mechanical analysis tests of nylon composites were conducted on DMA Q800 TA Instruments in tension mode at a heating rate of 5 °C/min. Thermogravimetric analysis (TGA) was performed using a TA Instruments TGA 2950 from 30 to 800 °C for GO samples and from 30 to 600 °C for composites at a heating rate of 10 °C/min in nitrogen and air atmosphere, respectively. The chemical resistance of the nanocomposites was carried out by submerging the polymer film (used equal weight) into the hydrocarbon solvents and treated at 50 °C with continuous sonication. The changes in sample weight were measured at time intervals.

3. RESULTS AND DISCUSSION

The FTIR analysis was performed first to observe the evolution of the functional groups in GO during the modification process. Figure 2a shows the FTIR sprctrum of PEI-rGO. As can be seen from the FTIR spectrum of pure GO, owing to a large number of −COOH and −OH groups, a broad peak for −OH stretching appeared in the range of 3200−3640 cm^{-1}. Other characteristic peaks for C=O (keto, 1725 cm^{-1}), C=C bond (1624 cm^{-1}), C−OH stretching vibrations (1351 cm^{-1}), epoxy (1224 cm^{-1}), and C−O vibrations from alkoxy groups (1039 cm^{-1}) labeled in the figure are consistent with the data reported previously.[20,21] However, after modification of GO by PEI, some changes associated with some new absorption bands appeared. For PEI-rGO, the new absorption bands appearing at 1569 and 1648 cm^{-1} are assigned to C−NH (amide II) and HNC=O (amide I) stretching vibrations.[22] Another interesting observation was that the band at 1722 cm^{-1} for −C=O disappeared with the concurrent appearance of new amide carbonyl groups, corresponding to the successful amidation reaction between GO and PEI through which carboxylic acid groups of GO were substituted. The N−H stretching band of PEI is observed at 3272 cm^{-1}. In addition, peaks that appeared at 1452 and 1224 cm^{-1} were also attributed to the absorption of −C−H bending and −C−N stretching, respectively.

XPS was conducted further to understand the surface changes in more detail, and the profiles are presented in Figure 2b. The left-hand side profile of Figure 2b demonstrates the deconvoluted high resolution C 1s peaks of GO, which consist of two main peaks at binding energies of 284.8 eV (C1) and 286.3 eV (C2) corresponding to the graphitic sp^2-hybridized carbon atoms (C=C) and hydroxyl, epoxy (C−OH/C−O−C) groups and two minor peaks at 287.4 eV (C3) and 288.9 eV
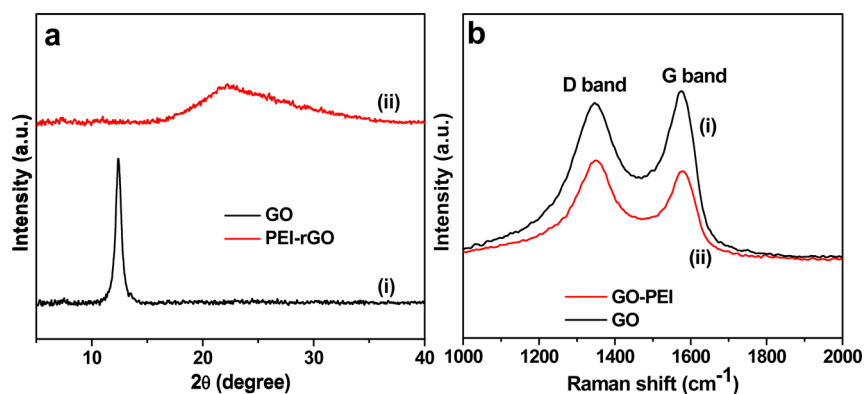
Figure 3. (a) XRD patterns and (b) Raman spectra of (i) GO and (ii) rGO-PEI.

(C4) attributed to the carbonyl (C═O) and carboxyl (O─C═O) groups, respectively.[20,23] However, after modification some distinct changes in the binding energy and intensity of C 1s spectrum of PEI-rGO were noticed.

The peak for ─COOH (288.9 eV) completely disappeared, while a new peak emerged at a binding energy of 288.4 eV which corresponded to the peak of amide (O═C─NH) as a result of amidation reaction. Moreover, the intensity of all oxygenated groups was significantly reduced which corroborated the effective chemical reduction of GO. These results clearly demonstrated the occurrences of simultaneous reduction and modification of GO by PEI.

Figure 3a and Figure 3b show the XRD patterns and Raman spectra of the GO and PEI-rGO, respectively. As expected, a typical sharp peak at 12.4° (d-spacing of ∼0.71 nm) was observed for pure GO powder. After it was treated with PEI, the characteristic peak of GO disappeared and a broad peak ranging from 16° to 30° was observed on the curves of PEI-rGO, which were ascribed to the reduction and restacking of the GO sheets. Figure 3b shows the Raman spectra of pure GO and PEI-rGO. As can be seen, both materials possesses D and G peaks at 1350 and 1583 cm^{-1} corresponding to the first-order scattering of the E_{2g} mode and structural disorder created by the surface functional groups, respectively. The I_D/I_G ratio of GO and PEI-rGO was measured to be 0.90 and 1.16, respectively. The increase in the above ratio of PEI-rGO suggested that the modification process altered the structure of GO through the formation of more sp^3 carbon.

The TGA profiles of GO, PEI, and PEI-rGO are discussed next in Figure 4. TGA was performed not only to estimate the amount of attached PEI but also to know the thermal behavior of the modified GO. In accordance with previous reports in refs 2, 10, and 24 the pure GO in our study also shows very low thermal stability and starts to lose mass at about 150 °C followed by a major loss at around 172–176 °C, presumably due to the loss of oxygen containing functional groups attached to the graphene sheets. On the contrary, the PEI modified rGO showed much higher thermal stability with 5% weight loss at 247 °C and 40% loss at 429 °C. As for the neat PEI, 100% weight loss can be seen below 400 °C.

Next, in order to find the impact of the PEI-rGO in the area of polymer composites, it was melt-blended with nylon 12 matrix and the mechanical, dynamic mechanical, and thermal properties of the resulting composites were evaluated. Typically a small amount, i.e., 0.25 and 0.35 wt % PEI-rGO, was incorporated into nylon matrix. The dynamic mechanical response of the nanocomposites is shown in Figure 5. Figure 5a
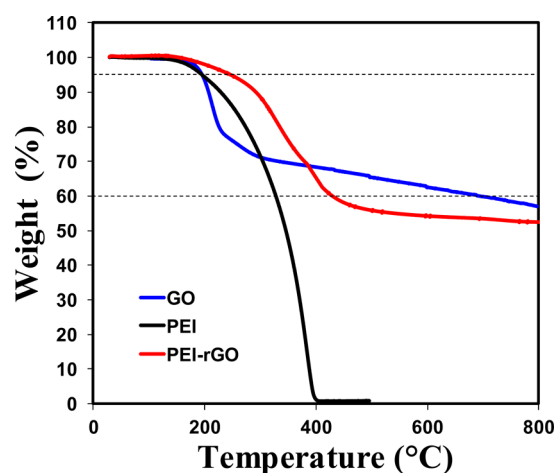

Figure 4. TGA curves of GO, PEI, and rGO-PEI.

and Figure 5b show the storage modulus (E') curves and loss angle tangent (tan δ) of the neat nylon 12 and nylon 12/PEI-rGO nanocomposites with respect to temperature. As can be seen, the storage modulus of pure Nylon within the set temperature range (30–185 °C) is considerably lower than that of the nanocomposites. After incorporation of GO, no matter raw or modified, the storage modulus of the nanocomposites is increased noticeably. Nevertheless, the storage modulus of the PEI-rGO containing nylon 12 nanocomposites showed much higher values as compared to the composite containing raw GO. Moreover, gradual improvement in storage modulus was obtained with increasing the PEI-rGO content from 0.25 to 0.35 wt %. It was also observed that nanocomposites containing 0.25 wt % PEI-rGO have much higher storage modulus value than the analogous raw GO nanocomposite and the degree of increment was found to be approximately 13% higher. At the initial temperature (0 °C), the storage modulus was 1514 MPa for pure nylon matrix and it reached the ultimate value of 2466 MPa, a 63% increase with addition of only 0.35 wt % PEI-rGO. This can be ascribed to the formation of strong interface interactions between the nylon 12 molecular chains and PEI-rGO and the inherent reinforcing effect imparted by the graphene. Moreover, the branched structure of PEI provides additional effect on the interface adhesion between the matrix and fillers through cross-linking and entanglement, leading to large mechanical strength of the nanocomposites. It can be seen that as the temperature increases, the storage modulus drops, indicating energy dissipation which occurs during the transition of the glassy state to a rubbery state. For pure nylon 12, the
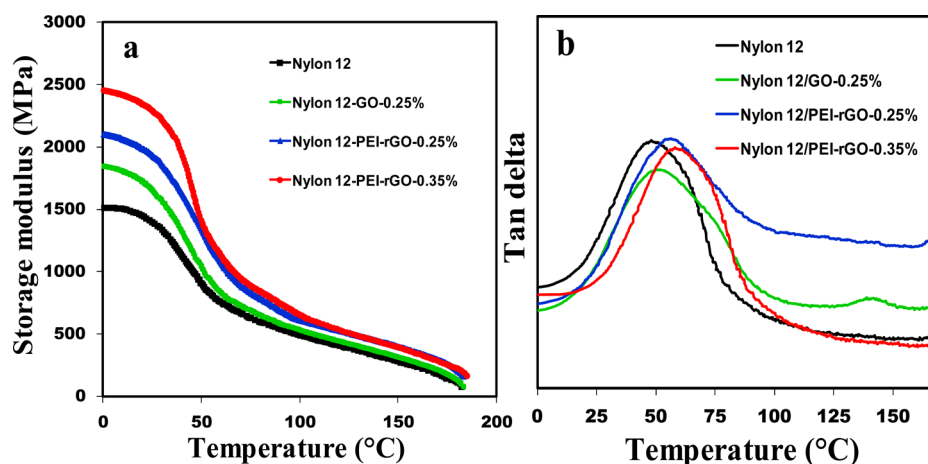
Figure 5. (a) Storage modulus and (b) tan δ as a function of temperature for pure nylon 12 and its graphene nanocomposites.

Table 1. Dynamic Mechanical and TGA Results of Nylon 12 Composites

sample	storage modulus (MPa)	% increment	tan δ/(T_g)	decomposition temp from TGA	
				T_5 (°C)	T_{50} (°C)
nylon 12	1514	-	48.20	414	453.1
nylon 12/0.25 wt % GO	1835	21.2	50.90	415.4	456.3
nylon 12/0.25 wt % PEI-rGO	2105	39.0	55.50	420.1	460
nylon 12/0.35 wt % PEI-rGO	2466	62.8	56.30	428.9	466.9

energy dissipation begins at around 22−25 °C which can also be seen from the tan δ curves (Figure 5b). It was also observed from the tan δ curves that incorporation of graphene oxide shifted the T_g of nylon 12 to the higher temperature side. The T_g increased from 48.2 °C for the pure nylon 12 to ∼50.9, 55., and 56.3 °C for the 0.25 wt % raw GO, 0.25 wt % PEI-rGO, and 0.35 wt % PEI-rGO nanocomposites, respectively.

The increase in T_g for the nanocomposites clearly demonstrates that the mobility of nylon chains in the matrix is confined by the GO as a result of strong filler/matrix interaction. This was more obvious for the nylon 12/PEI-rGO nanocomposites because of greater interactions owing to the branched structure of PEI that has more free amine groups to interact with amides in nylon (H-bonding interaction) caused by the excellent dispersion of the graphene nanosheets within the matrix. The details of the results are also presented in Table 1.

Figure 6 shows the stress−strain curves of the nylon 12 and the nanocomposites. As expected, the tensile strength of nylon 12/raw GO nanocomposite increases compared to the neat nylon 12 matrix, because of good interfacial interaction between the nylon 12 chains and surface functional groups on GO. However, dramatic enhancement in the tensile strength and Young's modulus (E) was obtained by addition of PEI-rGO into nylon 12, and it increases with increasing the PEI-rGO content. As can be seen from Table 2, the incorporation of only 0.35 wt % PEI-rGO radically increased the tensile strength and Young's modulus of the nanocomposites to 75.07 and 801 MPa, respectively, corresponding to an increase of 54% and 74% higher than that of the neat nylon 12. Such large improvement in the overall mechanical properties of the nylon 12/PEI-rGO nanocomposites can be attributed by many factors: (i) strong interfacial adhesion between the polymer chains and the modified graphene nanosheets, (ii) effective stress transfer from the polymer matrix to the graphene nanosheets, and (iii) excellent dispersion of the graphene
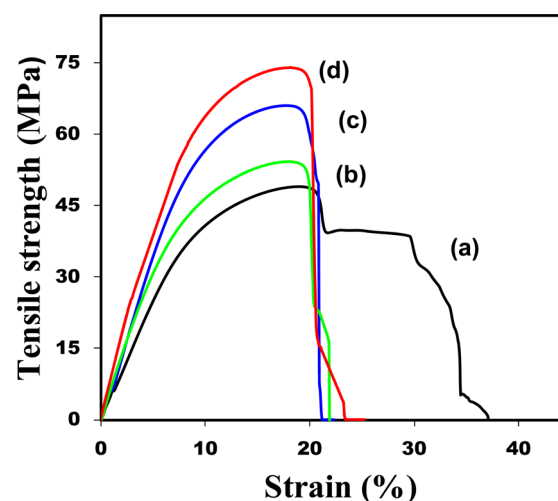

Figure 6. Tensile stress−strain curves of (a) pure nylon 12, (b) nylon 12/0.25 wt % GO, (c) nylon 12/0.25 wt % PEI-rGO, and (d) nylon 12/0.35 wt % PEI-rGO nanocomposites.

nanosheets throughout the polymer matrix. Another important reason could be that the PEI chains attached on graphene sheets may act as a spacer, leading to protection of the GO nanosheets from restacking by thermal reduction during melt blending and thereby improving its dispersion ability into the polymer matrix.

These strong interfacial interactions and excellent dispersion of PEI-rGO within nylon 12 matrix cause typical restriction in the movement of the polymer chains and are probably the reason for the lower elongation at break but higher Young's modulus as can be observed from the stress−strain curve. Nevertheless, the strength of our nanocomposites comprising such typically low loading of PEI-rGO is found to be much stronger than in many recent reports[10−16] that have even higher

Table 2. Tensile Strength Results of Nylon 12 Composites

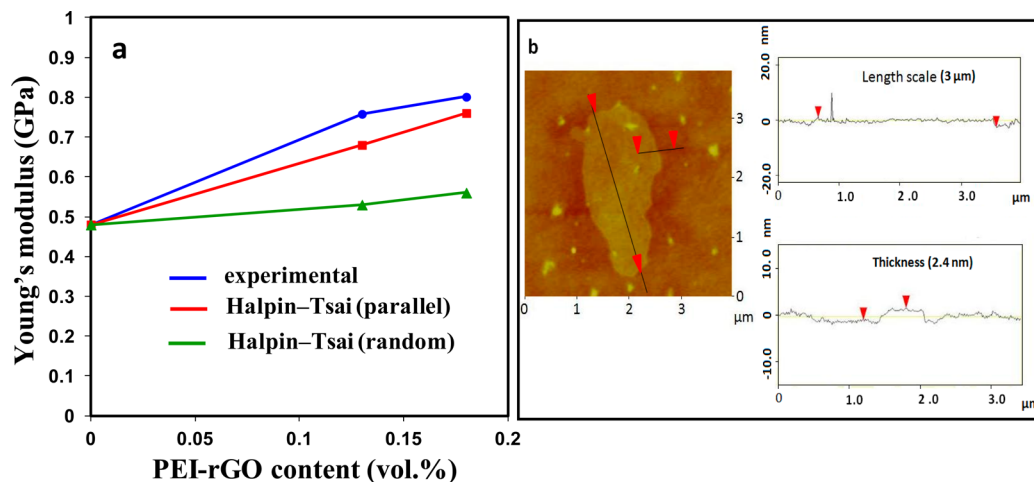| sample	tensile strength (MPa)	% increment	Young's modulus (MPa)	% increment
nylon 12	48.70 (±3.7)		460 (±16.8)	
nylon 12/0.25 wt % GO	54.22 (±3.9)	11.3	648 (±17.1)	40.8
nylon 12/0. 25 wt.% PEI-rGO	66.88 (±3.6)	37.3	758 (±17.6)	64.8
nylon 12/0.35 wt % PEI-rGO	75.07 (±4.0)	54.1	801 (±18.7)	74.1

Figure 7. Comparison between experimental Young's modulus data and theoretical values predicted by the Halpin−Tsai model for nylon 12/PEI-rGO nanocomposites. (b) AFM image of the PEI-rGO.

amount of graphene loading. It is worthwhile to mention that in order to avoid restacking and aggregations of graphene sheets as well as to attain full benefits in composite reinforcement, we optimized the formulation as stated above.

In order to further analyze the above mechanical properties, a comparison was made between the experimental results and the empirical model predictions for the composites as a function of the filler loading. The Halpin−Tsai model, which is the most widely used model[11,24−26] to estimate reinforcement effect of filler in composites, is considered here with the assumption that the GO sheets are aligned parallel or randomly to the surface of the nanocomposite films. This model provides a simple approximation of the Young's modulus of the composites based on the geometry and orientation of the filler as described by the following equations:[24,25]

$$E_{c\text{-random}} = E_{pm}\left[\frac{3}{8}\left(\frac{1 + (2l/3t)\eta_L V_g}{1 - \eta_L V_g}\right) + \frac{5}{8}\left(\frac{1 + 2\eta_T V_g}{1 - \eta_T V_g}\right)\right] \quad (1)$$

$$E_{c\text{-parallel}} = E_{pm}\left[\frac{1 + (2l/3t)\eta_L V_g}{1 - \eta_L V_g}\right] \quad (2)$$

$$\eta_L = \frac{\left(\frac{E_G}{E_{pm}}\right) - 1}{\frac{E_G}{E_{pm}} + 2l/(3t)} \quad (3)$$

$$\eta_T = \frac{\left(\frac{E_G}{E_{pm}}\right) - 1}{\frac{E_G}{E_{pm}} + 2} \quad (4)$$

where $E_{c\text{-random}}$ and $E_{c\text{-parallel}}$ are Young's modulus of the composites with randomly and parallel oriented graphene

sheets. E_{pm} and E_G are the tensile modulus of the polymer matrix and graphene, respectively. l, t, and V_g are the length, thickness, and volume fraction of the modified graphene. The thickness and average length of our modified graphene nanosheets are measured to be about 2.4 nm and 3 μm from the atomic force microscopic (AFM) analysis (Figure 7b). The density and modulus of nylon 12 and PEI-rGO is 1.02 g cm^{-3} and ∼460 MPa, and 1.9 g cm^{-3} and ∼300 GPa, respectively. Young's modulus of PEI-rGO was considered as based on an approximate value within the given literature reports.[26−28] Since in our system we used wt %, it needs to be converted to volume (V_g) % for the calculation. This can be done using the below equation:

$$V_g\ (\%) = \left[\frac{\frac{\text{weight \% of filler}}{\text{density of filler}}}{\left(\frac{\text{weight \% of polymer}}{\text{density of polymer}}\right) + \left(\frac{\text{weight \% of filler}}{\text{density of filler}}\right)}\right] \times 100 \quad (5)$$

The E_c values of the nylon 12 nanocomposites are calculated using eqs 1−5 and are shown in Figure 7. As can be seen from the plot, the experimental E values greatly exceeded the model predictions. Similar results were also been reported by Morimune et al. and Huang et al.[29,30] Moreover, the experimental E values were found closer to the theoretical simulation results based on the hypothesis that graphene sheets are oriented parallel to the surface of the matrix. This can also be evident from the FESEM images of the morphology of nanocomposites. These uncomparable reinforcement effects in our system clearly reflect the successful and effective load transfer to the graphene sheets across the graphene−nylon 12 interface which is believed to be the collective effects of excellent molecular level dispersion, strong interface bonding, uniform alignment, and increased crystallinity as stated above.
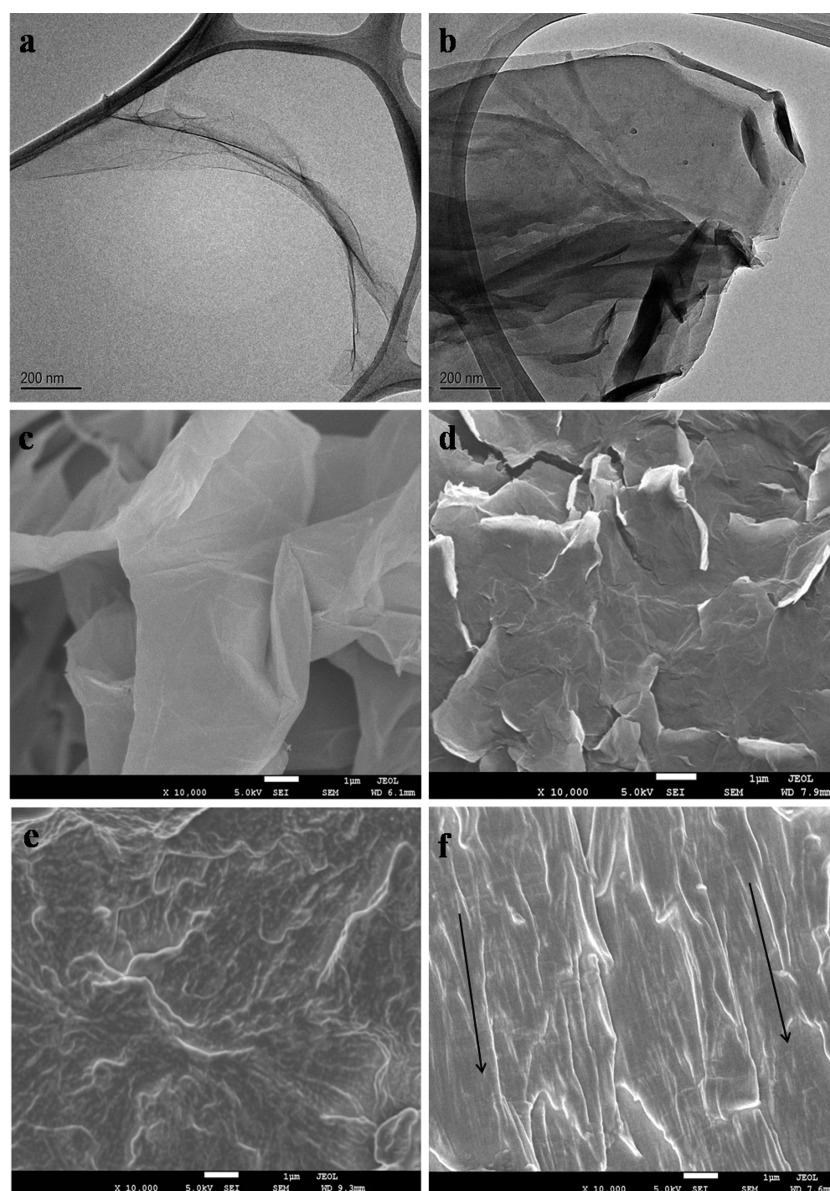
Figure 8. (a, b, c, d) TEM and FESEM images of GO and PEI-rGO, respectively. (e) Cross-sectional FESEM image of neat nylon 12 and (f) nylon 12/0.35 wt % PEI-rGO nanocomposite. Arrows shows the unidirectional orientation of graphene nanosheets.

Figure 8 demonstrates the typical morphology of pristine GO, PEI-rGO, and the cryo-fracture surface of the nano-composites. A clear difference in the morphological structure can be noticed between Figure 8a and Figure 8b which depicted the HRTEM images of pure GO and PEI-rGO samples, respectively. The surface of pure GO is found to be smooth, clean, and transparent, whereas after modification the surface of PEI-rGO becomes dark, corresponding to the attachment of polymer domains on the surface. The FESEM image also reveals the same fact. Compared to raw GO (Figure 8c), the FESEM image of PEI-rGO showed many wrinkles and ripples on the surfaces, attributed to the effect of successful surface modification by PEI. Such persistent wrinkle structures of modified graphene sheets have been reported to exhibit better interactions with the polymer matrix.[31,32] Figure 8e and Figure 8f show the fracture surface morphology of pure nylon 12 and 0.35 wt % PEI-rGO based nanocomposites. It is apparent that the fracture surface of pure nylon 12 is smooth, while the nanocomposites have rough surfaces due to tight embedding of

the PEI-rGO graphene nanosheets into the nylon matrix owing to the strong interfacial interactions between the PEI-rGO nanosheets and nylon 12 matrix. Moreover, the rough surfaces are also an indication of more energy absorption during fracture.

It can also be clearly seen from the FESEM image that the PEI-rGO nanosheets are uniformly distributed in the nylon matrix and aligned parallel to the surface of the film, which apparently endorses our above theoretical prediction for the calculation of Young's modulus based on the hypothesis that graphene sheets are oriented parallel to the surface of the matrix.

This uniform molecular level dispersion and alignment of PEI-rGO are probably the key factors for the above strikingly high mechanical strength of the nanocomposites even at extremely low loading (0.25 and 0.35 wt %). It is well-known to all that uniform distribution and orientation of fillers can render efficient stress transfer from the polymer matrix to the fillers through strong interfacial adhesion. However, the boundary

between the nylon matrix and the PEI-rGO is virtually indistinguishable to visualize, since the dispersed graphene nanosheets are covered by thick polymer layers.

The effect of various loadings of PEI-rGO on the hardness of nylon 12 composites was investigated by nanoindentation test method, and the typical loading−hold−unloading curves are presented in Figure 9. Each curve represents an average of 10
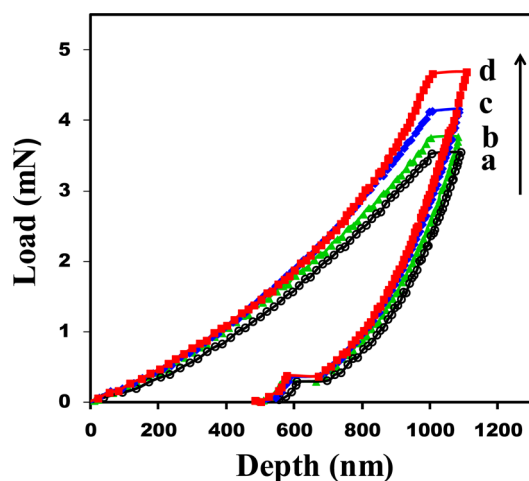

Figure 9. Typical loading−unloading curves (from nanoindentation measurement) of (a) pure nylon 12, (b) nylon 12/0.25 wt % GO, (c) nylon 12/0.25 wt % PEI-rGO, and (d) nylon 12/0.35 wt % PEI-rGO nanocomposites.

different measurements. From the profiles it can be immediately understood that PEI-rGO has a significant effect on the mechanical strength for nylon 12 composites. The nanohardness of unreinforced nylon 12 is 0.226 ($\pm$0.02) GPa, while for the 0.25 and 0.35 wt % PEI-rGO reinforced composites it increases to 0.235 and 0.242 GPa, respectively. The reduced modulus also increased from 2.59 GPa for nylon 12 to 2.67 and 2.73 GPa for the 0.25 and 0.35 wt % PEI-rGO reinforced nanocomposites. It can be seen that as a result of higher hardness the loading−unloading curves of the nano-composites dramatically moved to the upper side. The increase in nanohardness can be demonstrated with the dispersion effect of the modified graphene nanosheets. Furthermore, the creep resistance of the nanocomposites remained unaltered by addition of graphene, as seen by the same hold sections.

The TGA thermograms of the nanocomposites are illustrated next (Figure 10) to determine the thermal stability and the decomposition temperature. The decomposition temperatures at 5% (T_5) and 50% weight loss (T_{50}) are given in Table 1. It is interesting to observe that addition of such small amount of PEI-rGO, i.e., 0.25 and 0.35 wt %, can significantly alter the decomposition temperature of the nanocomposites to shift to the higher temperature side. As can be seen from both Table 1 and Figure 10, the addition of 0.35 wt % PEI-rGO into nylon 12 matrix increased the onset of degradation (defined by 5% weight loss) temperature of the composites by ~15 °C in comparison with the pure nylon 12. The 50% decomposition for the nylon 12/0.35 wt % PEI-rGO nanocomposites occurred at 466.9 °C which is ~14 °C higher than the pure nylon 12 (453.1 °C). The increase in thermal decomposition temper-ature of the nanocomposites can be attributed to the formation of a cross-linked network structure by PEI-rGO within the polymer matrix which can perform as an effective physical
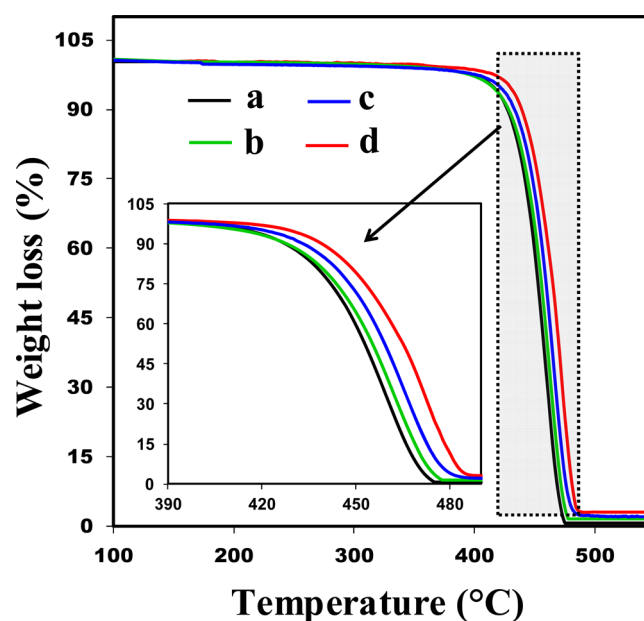

Figure 10. TGA curves of (a) pure nylon 12, (b) nylon 12/0.25 wt % GO, (c) nylon 12/0.25 wt % PEI-rGO, and (d) nylon 12/0.35 wt % PEI-rGO nanocomposites.

barrier to inhibit the release of the volatile products during combustion and the permeation of oxygen or air. Moreover, the uniform dispersion and alignment of graphene nanosheets within the network structure in the composites facilitate the increase of the mechanical integrity of the protective layer to hinder the evolution of the degradion products to the gas phase.

In addition, the strong interfacial interaction between nylon 12 chain and PEI-rGO can increase the activation energy of degradation and consequently increase the thermal stability of the composites.[33] Finally, the high thermal conductivity of graphene sheets can also facilitate the heat dissipation within composites and thereby improve the thermal stability of the composites. These results clearly demonstrate that precise control of the interface of graphene nanosheets can remarkably enhance the mechanical, dynamic-mechanical, and thermal properties of the nanocomposites by means of increasing the interlayer graphene exfoliation, molecular level dispersion, and matrix−filler interface adhesion at typically low loading.

When the chemical resistance property of the nano-composites was studied in various hydrocarbon solvents such as toluene, hexane, and paraffin oil, the nanocomposites exhibited exceptionally good chemical resistance. Figure 11 demonstrated the changes in weight over the time of immersion of the pure nylon 12 and nylon 12/0.35 wt % PEI-rGO composite into the above solvents. From our preliminary study it is apparent that incorporation of PEI-rGO can remarkbly increase the chemical barrier property of the nylon 12 matrix by reducing the permeability of toluene, paraffin oil, and hexane. As a result, no noticeable changes in weight gain of the nanocomposites were observed even after 24 h of treatment at 50 °C. The key factors of such improvement in the barrier properties can be explained by the platelet shape of the graphene nanosheets, their homogeneous distribution, and uniform alignment parallel to the direction of the film surface as demonstrated in FESEM analysis. This as a whole retards the propagation of the organic solvents molecules to
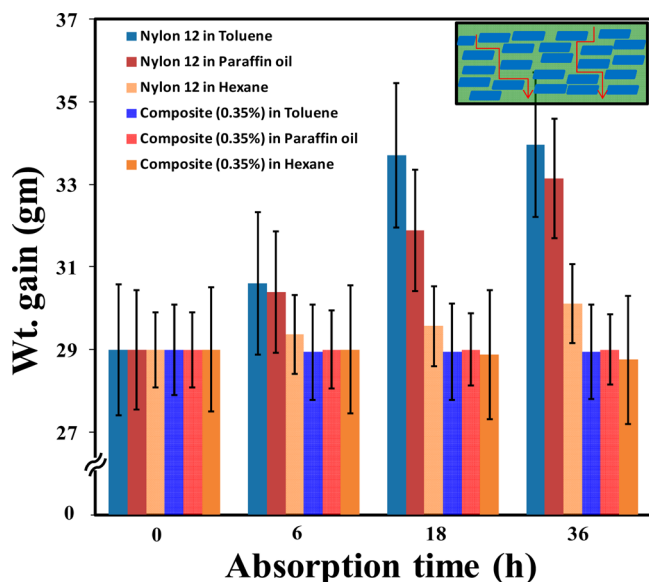
Figure 11. Time dependent solvent absorption of pure nylon 12 and its nanocomposites. All samples were treated at 50 °C. Inset shows the barrier properties of solvent permeation through the nanocomposites.

travel directly through the nylon matrix, which in turn results in lengthening of the travel path of the solvent molecules (see the inset in Figure 11) across the nanocomposite thickness. On the basis of the above findings, we certainly believe that these composite materials can be used for various applications such as (i) coating or jacketing material on various cables such as optical fibers, anti-termite cables, rat bite resistant cables due to its excellent mechanical strength, and surface hardness, (ii) liner material in specific oil-line applications such as diesel tubes, tubes for central greasing systems, and chemical vapor tubes for various automotive engine parts due to its good chemical resistance properties.

4. CONCLUSIONS

In this article, a novel strategy has been reported to functionalize graphene oxide with highly reactive amine groups with the aim of fabricating robust polymer nanocomposites. The synthetic methodology used here not only is useful to produce large amounts of aminated graphene oxides but also provides reduced and exfoliated graphene sheets that are extremely desirable in the preparation of high-strength polymer composites. The formation of modified graphene oxide is confirmed by various techniques including FTIR, XPS, TGA, Raman, and XRD. The polymer nanocomposites fabricated using this particular graphene oxide showed remarkable improvement in the mechanical performance, which is believed to be the result of our selective functionalization strategy that offered extremely good interfacial bonding, excellent dispersion, and orientation. It has been found that addition of only 0.35 wt % PEI-rGO improved the tensile strength and Young's modulus by 54% and 74%, which are far superior to many recent reported values. The DMA results showed ∼63% enhancement in the storage modulus, while the glass transition temperature increased by 8 °C. The thermal stability of nylon 12 also significantly improved with the addition of PEI-rGO. In addition, the barrier properties of the nanocomposites increased drastically. Therefore, in conclusion it can be said that proper functionalization of graphene oxide is very important to capture the inherent incredible properties of graphene oxide for fabricating high-performance polymer composites.

■ AUTHOR INFORMATION

Corresponding Authors
*X.H.: e-mail: axshu@ntu.edu.sg; phone, +65 6790 4610.
*C.Y.Y.: e-mail, mcyyue@ntu.edu.sg.

Author Contributions
§S. Roy and X. Tang are equal-contributing authors.

Notes
The authors declare no competing financial interest.

■ REFERENCES

(1) Novoselov, K. S.; Geim, A. K.; Morozov, S. V.; Jiang, D.; Zhang, Y.; Dubonos, S. V.; Grigorieva, I. V.; Firsov, A. A. Electric Field Effect in Atomically Thin Carbon Films. *Science* **2004**, *306*, 666−669.

(2) Bao, C.; Guo, Y.; Song, L.; Kan, Y.; Qian, X.; Hu, Y. In Situ Preparation of Functionalized Graphene Oxide/Epoxy Nanocomposites with Effective Reinforcements. *J. Mater. Chem.* **2011**, *21*, 13290−13298.

(3) Liu, F.; Song, S.; Xue, D.; Zhang, H. Folded Structured Graphene Paper for High Performance Electrode Materials. *Adv. Mater.* **2012**, *24*, 1089−1094.

(4) Liu, J.; Xue, Y.; Zhang, M.; Dai, L. Graphene-Based Materials for Energy Applications. *MRS Bull.* **2012**, *37*, 1265−1272.

(5) Tang, H.; Ehlert, G. J.; Lin, Y.; Sodano, H. A. Highly Efficient Synthesis of Graphene Nanocomposites. *Nano Lett.* **2012**, *12*, 84−90.

(6) Zhang, L. L.; Zhao, X.; Stoller, M. D.; Zhu, Y.; Ji, H.; Murali, S.; Wu, Y.; Perales, S.; Clevenger, B.; Ruoff, R. S. Highly Conductive and Porous Activated Reduced Graphene Oxide Films for High-Power Supercapacitors. *Nano Lett.* **2012**, *12*, 1806−1812.

(7) Shen, B.; Zhai, W.; Zheng, W. Ultrathin Flexible Graphene Film: An Excellent Thermal Conducting Material with Efficient EMI Shielding. *Adv. Funct. Mater.* **2014**, *24*, 4542−4548.

(8) Cai, D.; Song, M. Recent Advance in Functionalized Graphene/Polymer Nanocomposites. *J. Mater. Chem.* **2010**, *20*, 7906−7915.

(9) Terrones, M.; Martin, O.; Gonzalez, M.; Pozuelo, J.; Serrano, B.; Cabanelas, J. C.; Vega-Diaz, S. M.; Baselga, J. Interphases in Graphene Polymer-Based Nanocomposites: Achievements and Challenges. *Adv. Mater.* **2011**, *23*, 5302−5310.

(10) Fang, M.; Wang, K.; Lu, H.; Yang, Y.; Nutt, S. Covalent Polymer Functionalization of Graphene Nanosheets and Mechanical Properties of Composites. *J. Mater. Chem.* **2009**, *19*, 7098−7105.

(11) Liang, J.; Huang, Y.; Zhang, L.; Wang, Y.; Ma, Y.; Guo, T.; Chen, Y. Molecular-Level Dispersion of Graphene into Poly(vinyl alcohol) and Effective Reinforcement of Their Nanocomposites. *Adv. Funct. Mater.* **2009**, *19*, 2297−2302.

(12) Huang, T.; Lu, R.; Su, C.; Wang, H.; Guo, Z.; Liu, P.; Huang, Z.; Chen, H.; Li, T. Chemically Modified Graphene/Polyimide Composite Films Based on Utilization of Covalent Bonding and Oriented Distribution. *ACS Appl. Mater. Interfaces* **2012**, *4*, 2699−2708.

(13) Yuan, X. Y.; Zou, L. L.; Liao, C. C.; Dai, J. W. Improved Properties of Chemically Modified Graphene/Poly(methyl methacrylate) Nanocomposites via a Facile in-Situ Bulk Polymerization. *eXPRESS Polym. Lett.* **2012**, *6*, 847−858.

(14) Goncalves, G.; Marques, P. A. A. P.; Barros-Timmons, A.; Bdkin, I.; Singh, M. K.; Emami, N.; Gracio, J. Graphene Oxide Modified with PMMA via ATRP as a Reinforcement Filler. *J. Mater. Chem.* **2010**, *20*, 9927−9934.

(15) Park, O.-K.; Kim, S.-G.; You, N.-H.; Ku, B.-C.; Hui, D.; Lee, J. H. Synthesis and Properties of Iodo Functionalized Graphene Oxide/Polyimide Nanocomposites. *Composites, Part B* **2014**, *56*, 365−371.

(16) Rafiq, R.; Cai, D.; Jin, J.; Song, M. Increasing the Toughness of Nylon 12 by the Incorporation of Functionalized Graphene. *Carbon* **2010**, *48*, 4309−4314.

(17) Athreya, S. R.; Kalaitzidou, K.; Das, S. Mechanical and Microstructural Properties of Nylon-12/Carbon Black Composites: Selective Laser Sintering versus Melt Compounding and Injection Molding. *Compos. Sci. Technol.* **2011**, *71*, 506−510.

(18) Phang, I. Y.; Liu, T. X.; Mohamed, A.; Pramoda, K. P.; Chen, L.; Shen, L.; Chow, S. Y.; He, C. B.; Lu, X. H.; Hu, X. Morphology, Thermal and Mechanical Properties of Nylon 12/Organoclay Nanocomposites Prepared by Melt Compounding. *Polym. Int.* **2005**, *54*, 456−464.

(19) Khomenko, V.; Frackowiak, E.; Beguin, F. Determination of the Specific Capacitance of Conducting Polymer/Nanotubes Composite Electrodes Using Different Cell Configurations. *Electrochim. Acta* **2005**, *50*, 2499−2506.

(20) Yoo, M. J.; Kim, H. W.; Yoo, B. M.; Park, H. B. Highly Soluble Polyetheramine-Functionalized Graphene Oxide and Reduced Graphene Oxide Both in Aqueous and Non-Aqueous Solvents. *Carbon* **2014**, *75*, 149−160.

(21) Yu, Y.-H.; Lin, Y.-Y.; Lin, C.-H.; Chan, C.-C.; Huang, Y.-C. High-Performance Polystyrene/Graphene-Based Nanocomposites with Excellent Anti-Corrosion Properties. *Polym. Chem.* **2014**, *5*, 535−550.

(22) Yu, G.; Wu, P. Effect of Chemically Modified Graphene Oxide on the Phase Separation Behaviour and Properties of an Epoxy/Polyetherimide Binary System. *Polym. Chem.* **2014**, *5*, 96−104.

(23) Yang, Y.-K.; He, C.-E.; Peng, R.-G.; Baji, A.; Du, X.-S.; Huang, Y.-L.; Xie, X.-L.; Mai, Y.-W. Non-Covalently Modified Graphene Sheets by Imidazolium Ionic Liquids for Multifunctional Polymer Nanocomposites. *J. Mater. Chem.* **2012**, *22*, 5666−5675.

(24) Choudhury, A. Preparation and Characterization of Nanocomposites of Poly-*p*-phenylene Benzobisthiazole with Graphene Nanosheets. *RSC. Adv.* **2014**, *4*, 8856−8866.

(25) Carotenuto, G.; De Nicola, S.; Palomba, M.; Pullini, D.; Horsewell, A.; Hansen, T. W.; Nicolais, L. Mechanical Properties of Low-Density Polyethylene Filled by Graphite Nanoplatelets. *Nanotechnology* **2012**, *23*, 485705.

(26) Gomez-Navarro, C.; Burghard, M.; Kern, K. Elastic Properties of Chemically Derived Single Graphene Sheets. *Nano Lett.* **2008**, *8*, 2045−2049.

(27) Tombler, T. W.; Zhou, C. W.; Alexseyev, L.; Kong, J.; Dai, H. J.; Lei, L.; Jayanthi, C. S.; Tang, M. J.; Wu, S. Y. Reversible Electromechanical Characteristics of Carbon Nanotubes under Local-Probe Manipulation. *Nature* **2000**, *405*, 769−772.

(28) Lee, C.; Wei, X.; Kysar, J. W.; Hone, J. Measurement of The Elastic Properties and Intrinsic Strength of Monolayer Graphene. *Science* **2008**, *321*, 385−388.

(29) Morimune, S.; Nishino, T.; Goto, T. Poly(vinyl alcohol)/Graphene Oxide Nanocomposites Prepared by a Simple Eco-Process. *Polym. J.* **2012**, *44*, 1056−1063.

(30) Huang, T.; Xin, Y.; Li, T.; Nutt, S.; Su, C.; Chen, H.; Liu, P.; Lai, Z. Modified Graphene/Polyimide Nanocomposites: Reinforcing and Tribological Effects. *ACS Appl. Mater. Interfaces* **2013**, *5*, 4878−4891.

(31) Tang, L.-C.; Wan, Y.-J.; Yan, D.; Pei, Y.-B.; Zhao, L.; Li, Y.-B.; Wu, L.-B.; Jiang, J.-X.; Lai, G.-Q. The Effect of Graphene Dispersion on The Mechanical Properties of Graphene/Epoxy Composites. *Carbon* **2013**, *60*, 16−27.

(32) Ramanathan, T.; Abdala, A. A.; Stankovich, S.; Dikin, D. A.; Herrera-Alonso, M.; Piner, R. D.; Adamson, D. H.; Schniepp, H. C.; Chen, X.; Ruoff, R. S.; Nguyen, S. T.; Aksay, I. A.; Prud'homme, R. K.; Brinson, L. C. Functionalized Graphene Sheets for Polymer Nanocomposites. *Nat. Nanotechnol.* **2008**, *3*, 327−331.

(33) Yang, K.; Gu, M.; Han, H.; Mu, G. Influence of Chemical Processing on the Morphology, Crystalline Content and Thermal Stability of Multi-Walled Carbon Nanotubes. *Mater. Chem. Phys.* **2008**, *112*, 387−392.

■ NOTE ADDED AFTER ASAP PUBLICATION

This paper posted ASAP on January 30, 2015. A correction was made to the text in the Results and Discussion and the revised version was reposted on February 2, 2015.